

P.1.13 A CASE STUDY OF A ROSS ICE SHELF AIR STREAM EVENT: A NEW PERSPECTIVE

Daniel F. Steinhoff^{1,2*}, Saptarshi Chaudhuri¹, David H. Bromwich^{1,2}

¹Polar Meteorology Group
Byrd Polar Research Center
The Ohio State University
Columbus, Ohio

²Atmospheric Sciences Program
Department of Geography
The Ohio State University
Columbus, Ohio

1. INTRODUCTION

The Ross Ice Shelf Air Stream (RAS) is the name given to the semi-permanent wind regime that characterizes the climate of the Ross Ice Shelf in Antarctica. The RAS is a key component of low-level mass transport from Antarctica to mid-latitudes (Parish and Bromwich 1998), and southerly flow across the Ross Ice Shelf often affects weather conditions at McMurdo station (Seefeldt et al. 2003, Monaghan et al. 2005). The term “RAS” was first used in the Antarctic Regional Interactions Meteorology Experiment documentation (Antarctic RIME, Parish and Bromwich 2002), but the components that comprise the RAS are well documented.

Katabatic winds are a prominent feature of the Antarctic near-surface wind regime. Parish and Bromwich (1987), van Lipzig et al. (2004), and Parish and Bromwich (2007) illustrate winter climatological streamlines of near-surface flow over Antarctica, and find “confluence zones” of large-scale drainage flow of cold air from the continental interior to lower elevations. These confluence zones represent an enhanced supply of negatively buoyant air upstream. One such confluence zone occurs just upstream (southeast) of the Ross Ice Shelf, termed the Siple Coast confluence zone (Parish and Bromwich 1986, Bromwich and Liu 1996, Liu and Bromwich 1997). Warm signatures in the TIR imagery represent cold, bora-type katabatic winds draining from East Antarctica (Bromwich 1989). The horizontal propagation of katabatic wind signatures across great distances is supported by the synoptic-scale pressure gradient, usually resulting from cyclones over the Amundsen Sea.

Another component of the RAS is barrier winds. Barrier winds result from stably stratified air being forced up against a mountain barrier and lacking sufficient kinetic energy to cross the barrier. Mass accumulation along the barrier results in formation of a localized pressure gradient and eventual geostrophic adjustment so that flow is parallel to the barrier, with the barrier to the left of the wind in the Southern Hemisphere

Recent studies have attempted to integrate katabatic winds, barrier winds, and synoptic-scale forcing into the coherent structure that is the RAS (Parish et al. 2006, Seefeldt et al. 2007, Seefeldt and Cassano 2008). While source regions for the RAS are found in the confluence zone along Siple Coast and through glacier valleys along the Transantarctic Mountains, the spatial patterns and intensity of the RAS are largely controlled by cyclonic forcing. The RAS is a robust feature of the boundary layer, as the seasonal cycle of katabatic winds (Parish and Cassano 2003) is not found for the RAS, suggesting that large-scale forcing is significant. The RAS is often illustrated visually using TIR satellite imagery, specifically the propagation of warm signatures across the Ross Ice Shelf (e.g., Carrasco and Bromwich 1993). The association of warm TIR signatures with the RAS signature is the same as that inferred for katabatic wind propagation – that turbulence associated with the wind stream destroys any surface inversion over the ice shelf, resulting in a warm signature. Here, we present a case study analysis from April 2004 featuring a prominent RAS-like warm TIR signature in Moderate Resolution Imaging Spectroradiometer (MODIS) imagery. Multi-spectral MODIS imagery analysis, combined with automatic weather station (AWS) observations and AMPS forecast model output are used in the analysis.

2. DATA

For the time period of this case study, AMPS employs Polar MM5, a version of the fifth-generation Pennsylvania State University-NCAR Mesoscale Model (Grell et al. 1995) optimized for use in polar regions by the Polar Meteorology Group at the Byrd Polar

* *Corresponding author address:* Daniel F. Steinhoff, Polar Meteorology Group, Byrd Polar Research Center, The Ohio State University, 1090 Carmack Road, Columbus, OH 43210.
Email: steinhoff@polarmet1.mps.ohio-state.edu

Research Center, The Ohio State University (Bromwich et al. 2001, Cassano et al. 2001). AMPS output used in this case study is at 30-km resolution, on a grid domain covering Antarctica and much of the surrounding Southern Ocean. There are 31 vertical half-sigma levels, with 11 levels in the lowest 1000 m to capture the complex interactions in the planetary boundary layer. The initial and boundary conditions are derived from the National Centers for Environmental Prediction Global Forecasting System (GFS) model.

Surface observations are obtained from the Antarctic Meteorological Research Center (AMRC) at the University of Wisconsin-Madison (UW) (<http://amrc.ssec.wisc.edu>). Temperature, wind speed, and wind direction observations at a height of 3 m are used. UW-AWS observations are instantaneous at a 10-minute frequency. Further information regarding UW automatic weather stations can be found in Stearns et al. (1993).

MODIS imagery from the Terra and Aqua satellites of the Earth Observing System (EOS) at 1 km resolution is obtained from the Level 1 and Atmosphere Archive and Distribution System website (LAADS Web, <http://ladsweb.nascom.nasa.gov/>) and processed using McIDAS software. MODIS band 31, at a wavelength of approximately 11.03 μm , is used for TIR imagery analysis. The MODIS Cloud Mask product (Ackerman et al. 1998), also obtained from LAADS Web, involves a battery of tests for cloud cover and clear sky conditions using brightness temperature differences between various infrared and visible channels to determine a level of confidence that MODIS is observing a clear-sky scene.

3. 0620 UTC 5 APRIL 2004

The beginning of the RAS signature is represented in the thermal infrared (TIR) imagery at 0620 UTC 5 April 2004 in Fig. 1a. A warm signature emanates from the southern base of the Ross Ice Shelf northwestward, where it becomes less distinguishable west of 180°. Several means are used to determine the cloud structure of the TIR imagery in Fig. 1a. The MODIS Cloud Mask product at 0620 UTC 5 April is shown in Fig. 1b. The region just south of the Ross Ice Shelf and along the southern tip (Amundsen Coast) is flagged as cloudy in the cloud mask. From interpretation of the TIR image this seems reasonable, although the cloud appears to be of a “scattered” nature. Except for the very southern section of the Ross Ice Shelf and portions of the western coast south of Nimrod Glacier, most of the Ross Ice Shelf is cloud-free, and the warm signature extending across the ice shelf is a surface feature. The signatures in the TIR imagery reflect the influence that wind speed has on near-surface temperature over the Ross Ice Shelf. Weak winds result in the formation of a near-surface temperature inversion, as air just above the surface cools radiatively during the polar night. Increased near-surface wind speeds result in turbulent

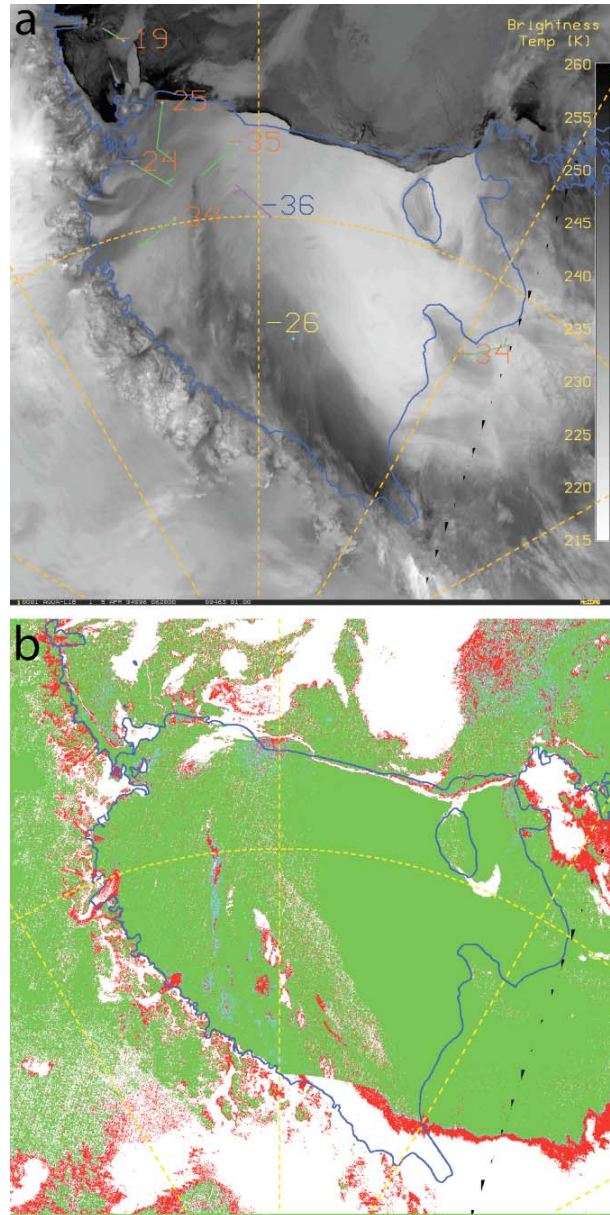


Figure 1. a) MODIS TIR image at 0620 UTC 5 April 2004 and selected AWS observations of near-surface air temperature and vector wind at 0600 UTC 5 April 2004. Gill AWS represented by blue temperature and purple wind barb. Lettau AWS represented by yellow temperature. b) MODIS Cloud Mask product at 0620 UTC 5 April 2004. Green represents clear conditions, light blue is probably clear, white is cloudy, and red is uncertain.

motions that prevent a near-surface temperature inversion from forming, which is the case for regions of warmer signatures in TIR imagery.

To gauge the performance of AMPS in capturing the near-surface conditions that characterize the TIR imagery, comparisons are done at Lettau and Gill AWS

stations between observations and AMPS (nearest grid point, wind speed and temperature logarithmically interpolated to 3 m height). Between 0000 UTC and 1200 UTC 5 April at Lettau (Fig. 2a), observed wind speeds generally range between 6 and 14 m s⁻¹, and AMPS wind speeds are generally in the 5.5-8 m s⁻¹ range. Even with moderate wind speeds for both observed and model values, there is a 10-20°C cold bias in AMPS. AMPS temperatures do not change significantly after 1200 UTC 5 April, when observed wind speeds and temperatures both decrease markedly.

The cold bias in AMPS on early 5 April may be related to the Mellor-Yamada-Janjić (MYJ) PBL scheme (Janjić 1994) used in the model, which has a shallow ~ 10°C surface inversion when it is unlikely that such an inversion exists with the moderate wind speeds observed. Zilitinkevich et al. (2008) show that there is a threshold interval of Richardson number (Ri) values, 0.1 < Ri < 1.0, which separates strong mixing regimes (Ri < 0.1) from weak mixing regimes (Ri > 1.0). In the latter, under a stable stratification regime, turbulence is generally in the form of internal waves, which are capable of transporting momentum, but not heat (represented by large turbulent Prandtl number values and weak turbulent heat flux values). Therefore, thermal stratification is largely maintained. The PBL scheme is clearly not resolving the sharp transition between weak and strong mixing regimes, which is likely a function of the surface layer stability function for turbulent exchange (Lüpkes et al. 2008).

At Gill (Fig. 2b), in the center of the Ross Ice Shelf, AMPS overestimates wind speeds (about 6 m s⁻¹, compared to about 2 m s⁻¹ in observations), but AMPS temperatures compare well with observations. Between 0000 UTC and 1200 UTC 5 April, the relationship between near-surface wind speed and temperature described previously is clearly evident when comparing observations between Lettau and Gill. Higher observed wind speeds at Lettau result in warmer temperatures, whereas weak wind speeds at Gill allow for radiative cooling and colder temperatures. Figure 2b also shows a station pressure comparison between observations and AMPS at Gill. AMPS captures the general trend in pressure readings throughout the time period, with errors well under 5 hPa. This comparison is representative of conditions in the region of the RAS signature during the case study. The surface pressure time series reflects changes in total vertical column atmospheric mass. Hence, substantial errors in AMPS appear to be restricted to the lowest levels, under influence of the PBL scheme.

4. 0340 UTC 6 APRIL 2004

The RAS event being discussed evolves from the warm TIR signature at the southern end of the Ross Ice Shelf to the situation shown in Fig. 3a. A warm signature in the TIR imagery narrows from the

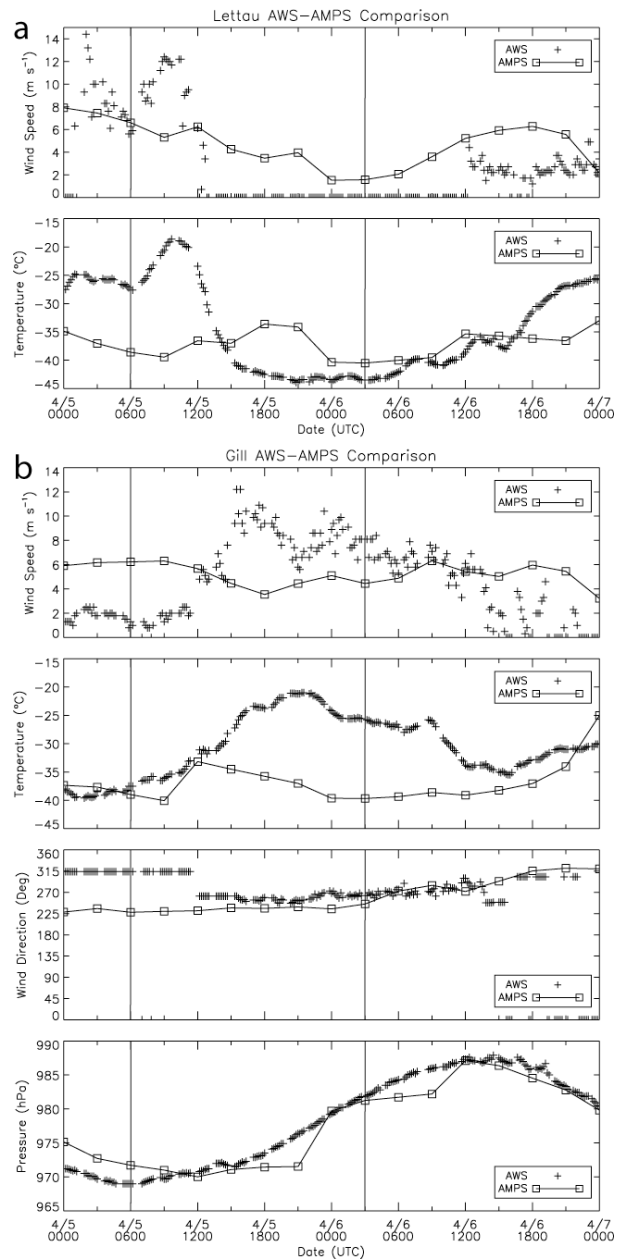


Figure 2. a) Lettau AWS and AMPS nearest-gridpoint comparisons of wind speed (top, m s⁻¹) and temperature (bottom, °C). b) same as a) except for Gill AWS wind speed, temperature, wind direction (degrees), and station pressure (hPa). Vertical lines represent conditions at image analysis times (0600 UTC 5 April and 0300 UTC 6 April).

southeastern edge of the image onto the Ross Ice Shelf. A well-defined warm signature extends northward along 180° over the Ross Ice Shelf, curving eastward towards the Ross Sea. As in the earlier image, a cold signature in the TIR imagery is located over most of the eastern section of the Ross Ice Shelf, between the warm signature and Roosevelt Island. Casual interpretation of

the Lettau and Gill wind and temperature observations in Fig. 3a and Fig. 2a-b indicates that the warm signature across the Ross Ice Shelf at this time is surface-based. Comparing Fig. 1a and Fig. 3a, it can be seen that Lettau AWS is within the warm signature at 0620 UTC 5 April and outside of it at 0340 UTC 6 April, while the reverse holds true for Gill AWS.

Correspondingly, Fig. 2a-b show that temperature and wind speed both decrease at Lettau AWS between images, while both increase at Gill AWS. Figure 4a shows AMPS wind speed and streamlines from $\sigma=0.9983$ (approx. 13 m AGL) at 0300 UTC 6 April. Weak wind speeds (under 6 m s^{-1}) are found over the central and eastern sections of the Ross Ice Shelf, corresponding with the cold signature in the TIR imagery, extending westward over portions of the warm TIR signature. However, streamlines near 80°S in Fig. 4a are almost normal to the warm signature in the TIR imagery. Additionally, the Gill wind direction observation shown in Fig. 3a is westerly, and is representative of observations in the hours leading up to and after this time (Fig. 2b). Based on the TIR imagery (Fig. 3a), AWS wind observations (Fig. 3a), and AMPS near-surface streamlines (Fig. 4a), the westerly winds near the surface appear to be of a katabatic origin. The warm signature in the TIR imagery appears to correspond better spatially with streamlines at $\sigma=0.9610$ (approx. 292 m AGL, Fig. 4b), suggesting that the warm TIR signature is not surface-based, but instead a low-level cloud. Figure 3b shows the MODIS Cloud Mask for 0340 UTC 6 April. The cloud region extending from the southern section of the Ross Ice Shelf near 180° to the north and east is flagged solely by the $11 \mu\text{m} - 3.9 \mu\text{m}$ BTD low cloud test.

As flow descends onto the Ross Ice Shelf, it accelerates in the lower levels along the Dufek Coast (Fig. 5a). The low-level jet feature in Fig. 5a features flow around the topography, rather than over, and hence is inferred to not be a tip jet, but instead “knob flow.” The knob flow phenomenon has been studied for flow around the Brooks Range on the northern coast of Alaska by Dickey (1961) and Kozo and Robe (1986). Figure 5a indicates deceleration of flow just downstream of the Dufek Coast. The jet offshore of the Dufek Coast and associated downstream deceleration are present in the lowest 750 m. Mass continuity dictates that the deceleration be accompanied by mass convergence and upward vertical motion. Figure 5b indicates that this is indeed the case, as there is a prominent region of upward vertical motion (up to about 18 cm s^{-1}) just downstream of the Dufek Coast at $\sigma=0.8971$ (approx. 790 m AGL). It is suggested that this region of upward vertical motion, combined with the low-level advection of moisture from the southeast, contributes to the development of low cloud over the Ross Ice Shelf.

Figure 6a-b shows cross sections of cloud ice mixing ratio and vertical velocity along line A-A' shown in Fig. 5. For the first image, a region of enhanced cloud ice at the leading edge of the cross section

appears to dissipate from the region of downward vertical motion near the Dufek Coast. A region of upward vertical motion is present just downstream of the Dufek Coast, similar to that found for the second image time in Fig. 5b. However, with low amounts of water vapor in the lower atmosphere, little cloud is formed in the region of upward vertical motion.

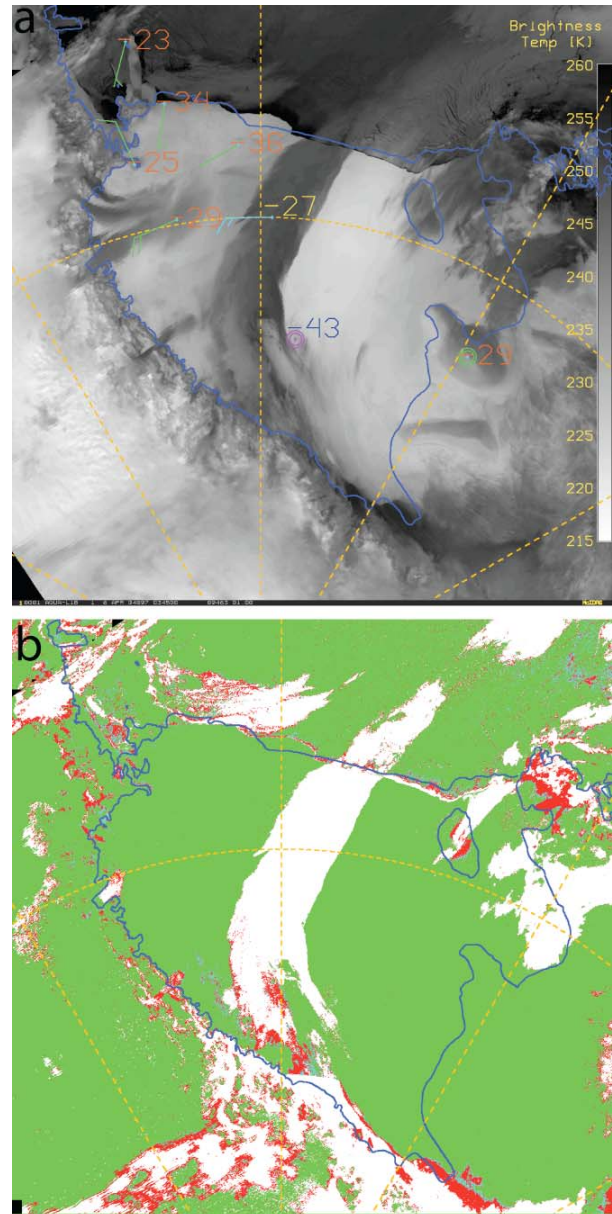


Figure 3. a) MODIS TIR image at 0340 UTC 6 April 2004 and selected AWS observations at 0400 UTC 6 April 2004. Gill AWS represented by yellow temperature and light blue wind barb. Lettau AWS represented by blue temperature and purple calm wind signal. b) MODIS Cloud Mask product at 0340 UTC 6 April 2004. Green represents clear conditions, light blue is probably clear, white is cloudy, and red is uncertain.

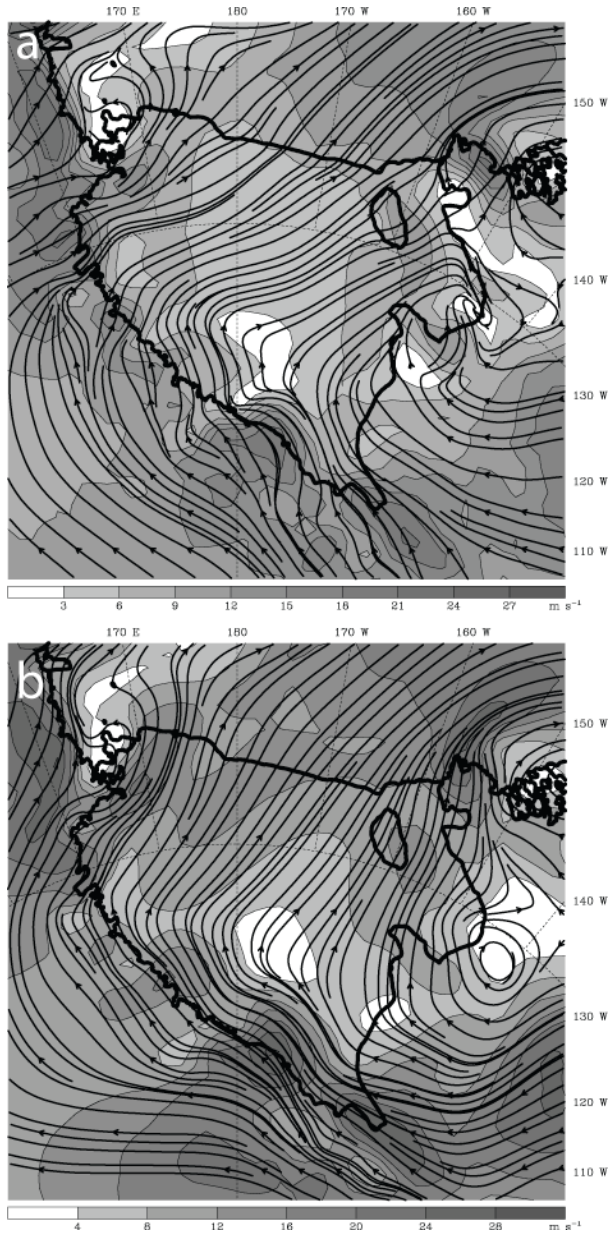


Figure 4. a) AMPS $\sigma=0.9983$ (approx. 13 m AGL) wind speed (shaded, $m s^{-1}$) and streamlines at 0300 UTC 6 April 2004. b) same as a) except for $\sigma=0.9610$ (approx. 292 m AGL).

In contrast to the first image time, maximum values of cloud ice mixing ratio are present between 3 and 4 km ASL for the second image time (Fig. 6b). The region of upward vertical motion shown in Fig. 6b is present from near the surface to a height of approximately 2.5 km ASL, with maximum values between 500 m and 1000 m ASL. Cloud ice development occurs just downstream of the upward vertical motion region in the lowest 2 km or so. It is likely that moisture-laden air advected onto the Ross Ice Shelf rises, cools, and

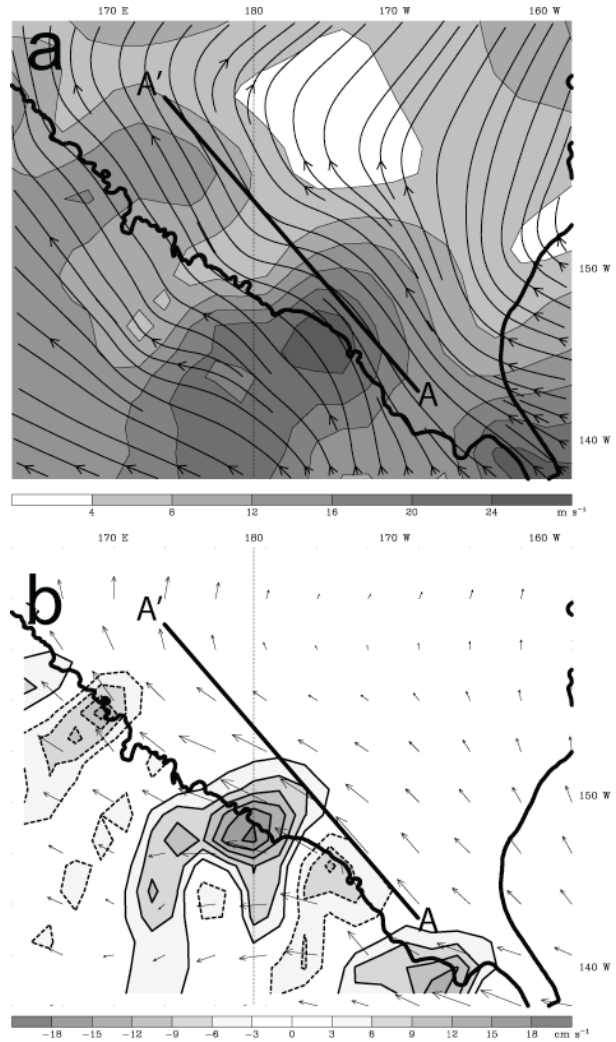


Figure 5. a) AMPS $\sigma=0.9791$ (approx. 216 m AGL) wind speed (shaded, $m s^{-1}$) and streamlines at 0300 UTC 6 April. b) AMPS $\sigma=0.8971$ (approx. 790 m AGL) vertical velocity (shaded, solid outline positive (upward vertical motion), dashed outline negative (downward vertical motion), $cm s^{-1}$) and wind vectors at 0300 UTC 6 April. Cross section line A-A' refers to Fig. 6.

condenses into ice cloud in association with the low-level upward vertical motion.

To illustrate the propagation of the low cloud across the ice shelf, Fig. 7a shows a trajectory analysis. Two separate trajectories (labeled "1" and "2" in Fig. 7a), chosen to represent the boundaries of the cloud signature in Fig. 3a, begin at $\sigma=0.9344$ (approx. 496 m AGL) for a southern and northern section in Fig. 7a, in order to best mimic conditions around 0300 UTC 6 April. The southern section begins at 2100 UTC 5 April and runs through 0600 UTC 6 April, and the northern section begins at 1800 UTC 5 April and runs through 0900 UTC 6 April. The combined trajectories form a pattern qualitatively similar to the warm signature in Fig. 3a.

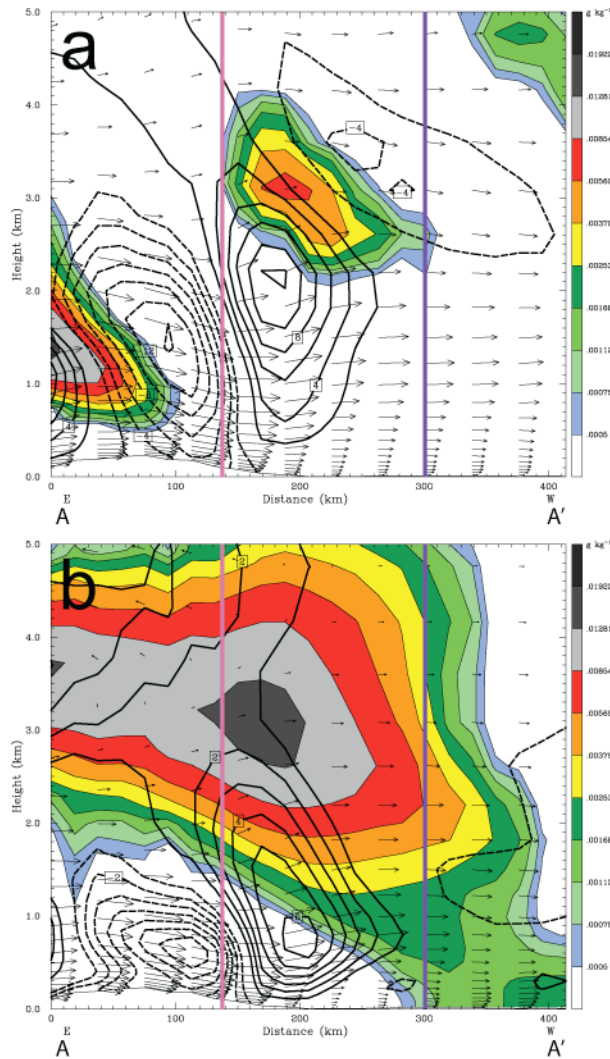


Figure 6. a) Cross section of cloud ice mixing ratio (shaded, $g\ kg^{-1}$), vertical velocity (contours, solid outline positive (upward vertical motion), dashed outline negative (downward vertical motion), $cm\ s^{-1}$, contour interval $2\ cm\ s^{-1}$), and circulation vectors at 0600 UTC 5 April 2004. b) same as a) except at 0300 UTC 6 April 2004. Cross section line shown in Fig. 5. Pink vertical line refers to approximate location of Dufek Coast. Blue vertical line refers to 180° .

Figure 7a shows that the flow across the Ross Ice Shelf allows for the cloud signature to retain a coherent spatial structure. Subsidence over northern portions of the ice shelf (not shown) traps moisture in the low-levels, preventing the cloud from “mixing out” vertically. Figure 7b shows height and relative humidity along the trajectories. For both trajectories, relative humidity increases in accordance with the upward vertical motion associated with low-level convergence downstream of the Dufek Coast (around 0000 UTC 6 April). RH remains well above 90% along the remainder of the southern section. For the northern section, relative

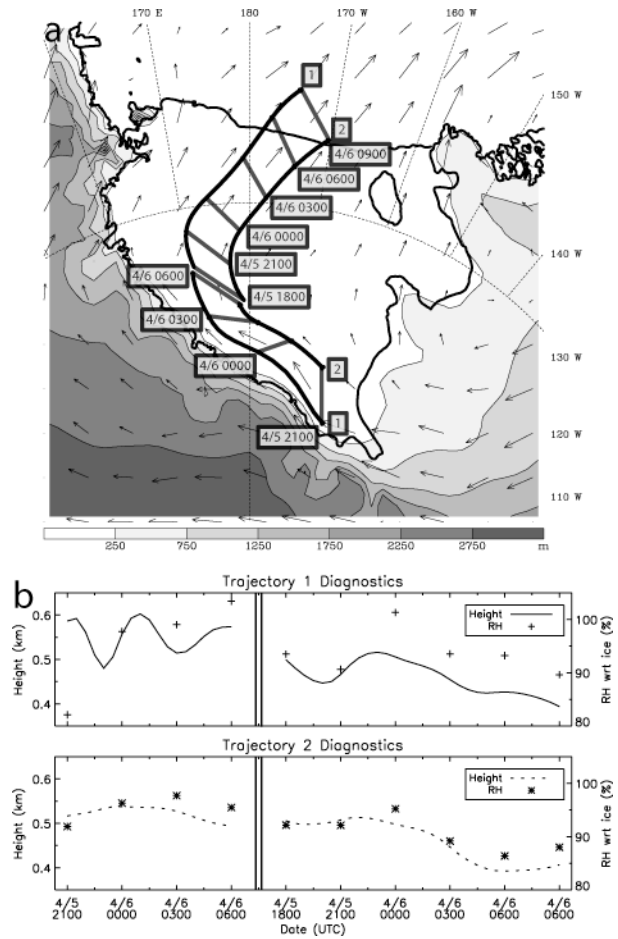


Figure 7. a) Trajectories beginning at $\sigma=0.9344$ (approx. 496 m AGL) from 2100 UTC 5 April to 0600 UTC 6 April (southern section) and 1800 UTC 5 April to 0900 UTC 6 April (northern section). Trajectories #1 and #2 labeled. Corresponding times between trajectories indicated by connecting dark gray bars. Wind vectors at $\sigma=0.9344$ at 0300 UTC 6 April, and terrain height shaded every 250 m. b) Trajectory 1 (top) and 2 (bottom) height (line, km) and relative humidity (RH) with respect to ice (symbol, %) for the northern and southern trajectory sections. Height interpolated to 30-minute intervals, RH output every 3 hours. Double bars separate southern and northern trajectory sets.

humidity values begin above 90%, and decrease to just under 90% by 0900 UTC 6 April as the trajectory descends.

5. CONCLUSIONS

A case is presented where a warm signature in TIR imagery across the Ross Ice Shelf, which resembles the near-surface signature of the RAS, is actually low-level cloud. Moisture is transported across West Antarctica from the Amundsen and Bellingshausen Seas, associated with a synoptic-scale cyclone centered near

the Marie Byrd Land coast. Cloud formation over the southern portion of the Ross Ice Shelf occurs in conjunction with a lifting mechanism formed by “knob flow” and associated downstream mass convergence at low levels. Trajectory analysis indicates that the signature retains a coherent spatial structure, and subsidence associated with a building upper-level ridge traps the cloud in the lower levels.

The results of this work show that the assumption used in previous RAS-related studies, that warm signatures in TIR imagery extending across the Ross Ice Shelf are solely surface features, may be incorrect. The benefit of an integrated approach to study of the RAS, combining satellite data, AWS observations, and model output is apparent from this analysis, as casual interpretation of AWS temperature and wind data in the context of the satellite signature suggests a surface feature is present throughout the analysis. Future efforts towards better understanding the RAS include an extension of the warm TIR signature analysis presented here to a longer time period in order to gain a firm grasp of the climatological context of this case. More detailed study of the individual atmospheric phenomena, in particular moisture transport across West Antarctica (not shown here) and dynamics of the Dufek Coast wind maximum, is desirable. In order to better simulate this event, not only would higher spatial resolution be beneficial, but also the use of a PBL scheme that accurately represents wind and temperature regimes over flat ice surfaces with weak forcing would be necessary.

A more detailed explanation of this work can be found in Steinhoff et al. (2009).

ACKNOWLEDGEMENTS

This research is supported by the National Science Foundation via UCAR subcontract S01-22901 and grant NSF-ANT-0636523 to DHB. Thanks go to Matthew Lazzara (SSEC / University of Wisconsin-Madison) who provided guidance with McIDAS and to Timo Vihma (FMI) for helpful discussions regarding model PBL issues.

REFERENCES

- Ackerman, S. A., K. I. Strabala, W. P. Menzel, R. A. Frey, C. C. Moeller, and L. E. Gumley, 1998: Discriminating clear-sky from clouds with MODIS. *J. Geophys. Res.*, **103 (D24)**, 32 141-32 157.
- Bromwich, D. H., 1989: Satellite analyses of Antarctic katabatic wind behavior. *Bull. Amer. Meteor. Soc.*, **70**, 738-749.
- , and Z. Liu, 1996: An observational study of the katabatic wind confluence zone near Siple Coast, West Antarctica. *Mon. Wea. Rev.*, **124**, 462-477.
- , J. J. Cassano, T. Klein, G. Heinemann, K. M. Hines, K. Steffen, and J. E. Box, 2001: Mesoscale modeling of katabatic winds over Greenland with the Polar MM5. *Mon. Wea. Rev.*, **129**, 2290-2309.
- Carrasco, J. F. and D. H. Bromwich, 1993: Satellite and automatic weather station analyses of katabatic surges across the Ross Ice Shelf. *Antarctic Meteorology and Climatology: Studies Based on Automatic Weather Stations*, D. H. Bromwich and C. R. Stearns, Eds., Antarctic Research Series, Vol. 61, American Geophysical Union, 93-108.
- Cassano, J. J., J. E. Box, D. H. Bromwich, L. Li, and K. Steffen, 2001: Evaluation of Polar MM5 simulations of Greenland's atmospheric circulation. *J. Geophys. Res.*, **106**, 33 867-33 889.
- Dickey, W. W., 1961: A study of a topographic effect on wind in the Arctic. *J. Meteorol.*, **18**, 790-803.
- Grell, G. A., J. Dudhia, and D. R. Stauffer, 1995: A description of the fifth-generation Penn State/NCAR Mesoscale Model (MM5). NCAR Tech. Note NCAR/TN-398+STR, 122 pp.
- Janjić, Z. I., 1994: The step-mountain eta coordinate model: Further developments of the convection, viscous sublayer, and turbulence closure schemes. *Mon. Wea. Rev.*, **122**, 927-945.
- Kozo, T. L., and R. Q. Robe, 1986: Modeling winds and open-water buoy drift along the eastern Beaufort Sea coast, including the effects of the Brooks Range. *J. Geophys. Res.*, **91**, 13 011-13 032.
- Liu, Z., and D. H. Bromwich, 1997: Dynamics of the katabatic wind confluence zone near Siple Coast, West Antarctica. *J. Appl. Meteorol.*, **36**, 97-118.
- Lüpkes, C., T. Vihma, G. Birnbaum, and U. Wacker, 2008: Influence of leads in sea ice on the temperature of the atmospheric boundary layer during polar night. *Geophys. Res. Lett.*, **35**, L03805, doi:10.1029/2007GL032461.
- Monaghan, A. J., D. H. Bromwich, J. G. Powers, and K. W. Manning, 2005: The climate of McMurdo, Antarctica, region as represented by one year of forecasts from the Antarctic Mesoscale Prediction System. *J. Climate.*, **18**, 1174-1189.
- Parish, T. R., and D. H. Bromwich, 1986: The inversion wind pattern over West Antarctica. *Mon. Wea. Rev.*, **114**, 849-860.

- , and —, 1987: The surface windfield over the Antarctic Ice Sheets. *Nature*, **328**, 51-54.
- , and —, 1998: A case study of Antarctic katabatic wind interaction with large-scale forcing. *Mon. Wea. Rev.*, **126**, 199-209.
- , and —, (Eds.), 2002: Ross Island Meteorology Experiment (RIME), detailed science plan, BPRC Misc. Ser. M-424, 39 pp., Byrd Polar Res. Cent., Ohio State Univ., Columbus.
- , and —, 2007: Reexamination of the near-surface airflow over the Antarctic continent and implications on atmospheric circulations at high southern latitudes. *Mon. Wea. Rev.*, **135**, 1961-1973.
- , and J. J. Cassano, 2003: The role of katabatic winds on the Antarctic surface wind regime. *Mon. Wea. Rev.*, **131**, 317-333.
- , —, and M. W. Seefeldt, 2006: Characteristics of the Ross Ice Shelf air stream as depicted in Antarctic Mesoscale Prediction System simulations. *J. Geophys. Res.*, **111**, D12109, doi:10.1029/2005JD006185.
- Seefeldt, M. W., and J. J. Cassano, 2008: An analysis of low-level jets in the greater Ross Ice Shelf region based on numerical simulations. *Mon. Wea. Rev.*, **136**, 4188-4205.
- , G. J. Tripoli, and C. R. Stearns, 2003: A high resolution numerical simulation of the wind flow in the Ross Island Region, Antarctica. *Mon. Wea. Rev.*, **131**, 435-458.
- , J. J. Cassano, and T. R. Parish, 2007: Dominant regimes of the Ross Ice Shelf surface wind field during austral autumn 2005. *J. Appl. Meteorol. Clim.*, **46**, 1933-1955.
- Stearns, C. R., L. M. Keller, G. A. Weidner, and M. Sievers, 1993: Monthly mean climatic data for Antarctic automatic weather stations. Antarctic Meteorology and Climatology: Studies Based on Automatic Weather Stations, D. H. Bromwich and C. R. Stearns, Eds., Antarctic Research Series, Vol. 61, American Geophysical Union, 93-108.
- Steinhoff, D. F., S. Chaudhuri, and D. H. Bromwich, 2009: A case study of a Ross Ice Shelf air stream event: A new perspective. *Mon. Wea. Rev.*, accepted.
- van Lipzig, N. P. M., J. Turner, S. R. Colwell, and M. R. van den Broeke, 2004: The near-surface wind field over the Antarctic continent. *Int. J. Climatol.*, **24**, 1973-1982.
- Zilitinkevich, S. S., T. Elperin, N. Kleerorin, I. Rogachevskii, I. Esau, T. Mauritsen, and M. W. Miles, 2008: Turbulence energetics in stably stratified geophysical flows: Strong and weak mixing regimes. *Quart. J. Roy. Met. Soc.*, **134**, 793-799.